Biophysical Journal
Article

Biophysical Society

Structural reorganization and relaxation dynamics of axially stressed chromosomes

Benjamin S. Ruben,[1,2,*] Sumitabha Brahmachari,[1] Vinícius G. Contessoto,[1] Ryan R. Cheng,[1,3] Antonio B. Oliveira Junior,[1] Michele Di Pierro,[4,5] and José N. Onuchic[1,6]

[1]Center for Theoretical Biological Physics, Rice University, Houston, Texas; [2]Biophysics PhD Program, Harvard University, Cambridge, Massachusetts; [3]Department of Chemistry, University of Kentucky, Lexington, Kentucky; [4]Department of Physics, Northeastern University, Boston, Massachusetts; [5]Center for Theoretical Biological Physics, Northeastern University, Boston, Massachusetts; and [6]Department of Physics and Astronomy, Department of Chemistry, Department of BioSciences, Rice University, Houston, Texas

ABSTRACT Chromosomes endure mechanical stresses throughout the cell cycle; for example, resulting from the pulling of chromosomes by spindle fibers during mitosis or deformation of the nucleus during cell migration. The response to physical stress is closely related to chromosome structure and function. Micromechanical studies of mitotic chromosomes have revealed them to be remarkably extensible objects and informed early models of mitotic chromosome organization. We use a data-driven, coarse-grained polymer modeling approach to explore the relationship between the spatial organization of individual chromosomes and their emergent mechanical properties. In particular, we investigate the mechanical properties of our model chromosomes by axially stretching them. Simulated stretching led to a linear force-extension curve for small strain, with mitotic chromosomes behaving about 10-fold stiffer than interphase chromosomes. Studying their relaxation dynamics, we found that chromosomes are viscoelastic solids with a highly liquid-like, viscous behavior in interphase that becomes solid-like in mitosis. This emergent mechanical stiffness originates from lengthwise compaction, an effective potential capturing the activity of loop-extruding SMC complexes. Chromosomes denature under large strains via unraveling, which is characterized by opening of large-scale folding patterns. By quantifying the effect of mechanical perturbations on the chromosome's structural features, our model provides a nuanced understanding of in vivo mechanics of chromosomes.

SIGNIFICANCE How chromosomes, at various stages of the cell cycle, respond to physical stress is closely connected to their structure and function. Such stresses may originate from the pulling of chromosomes by spindle fibers during mitosis or deformation of the nucleus during cell migration. We use molecular dynamics simulations to quantitatively characterize the physical state of chromosomes throughout the cell cycle, finding good agreement with existing experimental observations. We show that large-scale structural features play a significant role in determining chromosome elasticity. Applied tension reorganizes chromosomes by disrupting chromatin compartments in interphase and lengthwise compaction in mitosis, yielding distinct, testable experimental signatures. Our results will aid in interpreting future experiments studying mechanical perturbations of chromosomes.

INTRODUCTION

Understanding the physical nature of chromosomes is an outstanding challenge in modern biology. The mechanical properties of chromosomes are relevant to their biological function. For example, when chromosomes are pulled and manipulated by spindle fibers during mitosis, mechanical robustness to stretching is essential to preserve chromosome integrity. Recent experiments have probed the mechanical response of individual chromatin loci subjected to an externally applied force (1), revealing that interphase chromatin is highly dynamic and liquid-like. Other experiments probing chromatin mobility have given evidence that chromatin is arranged in a solid-like gel state (2). It has further been shown that intact chromatin is needed to maintain the structural integrity of the whole nucleus (3) and that the mechanical responsiveness of the nucleus is modulated through heterochromatin formation (4).

The mechanical properties of mitotic chromosomes have been probed directly in experiments that use micromanipulation to stretch individual chromosomes and measure their

Submitted September 13, 2022, and accepted for publication March 17, 2023.

*Correspondence: benruben@g.harvard.edu

Editor: Tamar Schlick.

https://doi.org/10.1016/j.bpj.2023.03.029

force-extension curves (5–10). Experiments have demonstrated that mitotic chromosomes extracted from live cells are highly extensible objects, maintaining their shape and native elasticity after being stretched up to five times their native length. Mitotic chromosomes display a linear force response in accordance with Hooke's law for extensions up to 40 times their native length, followed by a force plateau (5). Toward understanding the origin of chromosomal elasticity, several studies have explored how treatment of mitotic chromosomes with cleavage enzymes affects their mechanical properties (7,11). It was found that the elasticity of mitotic chromosomes was softened when treated with protease (11), which cleaves peptide bonds. However, the chromatin material disintegrated when treated with Micrococcal nuclease (7), which cleaves DNA. These findings suggested that the DNA molecule itself was principally responsible for the structural integrity and observed mechanical properties of a chromosome rather than any contiguous protein scaffold (7). For mitotic chromosomes assembled in vivo, measurements of the chromosome's bending modulus agree with the expected bending modulus for a linear elastic rod with the same elastic modulus and radius (7), suggesting that the mitotic chromosome's stiffness is distributed homogeneously over its cross section. Recent technological advances have allowed for measurement of human chromosome mechanics with high force-resolution, revealing a nonlinear stiffening behavior in the low strain regime (10).

Initial investigations of their mechanical properties led to the "chromatin mesh" model for mitotic chromosomes (5), which describes the mitotic chromosome as a mesh of extensible chromatin fibers cross-linked by a variety of factors, like the SMC proteins. However, a growing list of experimental results has since demonstrated that the mitotic chromosome should not be treated as a homogeneous material; in particular, (12) suggests that mitotic chromosome stretching occurs between rigid "condensin centers" placed discontinuously along the chromosome's length and (10) shows that TOP2A, another chromatin cross-linking protein, is not uniformly distributed along the mitotic chromosome's length, leading to non-uniform stretching. In addition, recent super-resolution microscopy experiments have demonstrated that mitotic chromosomes are organized into 80 kb domains that remain intact when chromosomes are stretched to even 30 times their native length (13). These findings suggest that the chromatin mesh model's explanation of chromosome elasticity is incomplete. It has been pointed out that at least part of the chromosomal elasticity may arise from the opening of large-scale chromatin folding (14) and hierarchical folding (10).

While early micromechanical studies have offered some insights into the internal organization of chromosomes, a revolution in conformation capture technology has since produced a wealth of new information about chromosome organization (15–20). In particular, Hi-C generates "contact maps" of the genome, which report the frequency with which any pair of genomic loci are observed to be spatially proximal. This technique allowed the discovery of rich structural motifs in the organization of the interphase nucleus, such as compartments and loops (15,17,21). Hi-C-based studies suggest that chromosome organization in the interphase nucleus is intricately connected to the regulation of gene expression (22). More recently, Hi-C has been applied to synchronous cell lines throughout mitotic cell division, to find that chromosome organization changes drastically when chromosomes are compacted into rod-shaped mitotic chromosomes (23,24). In particular, TADs and chromatin compartments disappear while SMC complex-driven chromatin looping (leading to lengthwise compaction) increases.

We previously introduced the Minimal Chromatin Model (MiChroM) (25), a data-driven, coarse-grained polymer model for chromosomes, which uses the principle of maximum entropy to infer an energy landscape for chromosome folding from Hi-C contact maps. MiChroM has been shown to quantitatively recapitulate the rich patterns of contact observed in Hi-C experiments. Structural ensembles generated by MiChroM provided new insights into interphase chromosome organization through the interplay between phase separation of biochemically distinct segments of chromatin (compartmentalization) and the genomic distance-dependent lengthwise compaction attributed to the activity of motors such as condensin and cohesin (called the ideal chromosome potential) (25–31). MiChroM has been shown to be consistent with locus-locus distance distributions determined with fluorescence in situ hybridization (25,32) and the dynamical viscoelasticity of chromosomes observed experimentally (33). Recent work has also shown MiChroM structures to be consistent with the structures observed in DNA-tracing experiments (34–36).

In this work, we study the relationship between a chromosome's large-scale organization and its mechanical properties using computer simulations of chicken (DT40) chromosomes in interphase and in mitosis. Model parameters were fit so that simulated contact maps are consistent with experimental Hi-C maps of interphase (G2) and mitotic (prometaphase) chromosomes of the DT40 cell line (23). First, we test the mechanical properties of the chromosome with in silico measurements of its force-extension curve and bending rigidity. We observe a linear elastic response in the low-extension regime, with a spring constant that increases 10-fold from interphase to mitosis (Fig. 1). The simulated chromosomes are found to unravel when chromosome extension reaches roughly double its native length, causing a plateau in their force-extension curves. The measured persistence length of 2.4 μm agrees with that expected for a homogeneous material, suggesting that stress is distributed evenly over the mitotic chromosome's cross section. Second, we investigate the dynamical

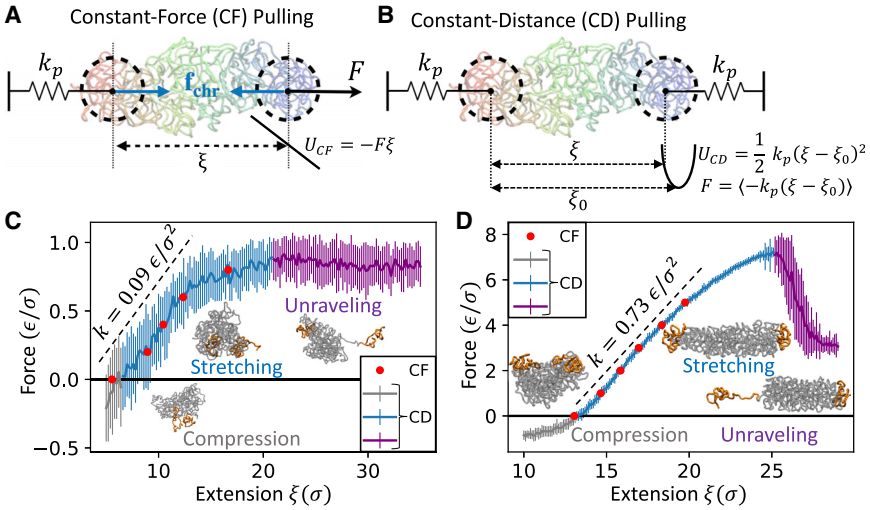

FIGURE 1 Force-extension behavior of simulated interphase and mitotic chromosomes. (*A*) Schematic representation of the constant-force (CF) simulation setup. The reaction coordinate for stretching is defined as the x-distance between the centers of mass of the pull groups ($\xi = x_r - x_l$). The pull groups are defined as the first and last 50 beads (2500 kb) of the chromosome. The center of mass of the left pull group (first 50 beads) is confined to the origin using a strong harmonic potential, and the right is constrained to the x axis but allowed to slide along it. Constant is applied through a linear pulling potential $U_{CF} = -F\xi$. (*B*) Schematic representation of constant-distance (CD) simulations. Setup is the same as CF simulations, except chromosome extension is restrained to a small window with a strong harmonic potential $U_{CD} = \frac{1}{2}k_p(\xi - \xi_0)^2$. Force is measured as the average restoring force of the applied restraining potential ($F = \langle -k_p(\xi - \xi_0)\rangle$). (*C* and *D*) Resulting force-extension curves for interphase/mitotic CF and CD measurements are overlaid. Force-extension curve for CD measurement is shown in gray, blue, and purple, corresponding to compression, stretching, and unraveling regimes, respectively. Error bars show the standard deviation of the mean force over 40 replica ensembles. Red circles show force-extension curves for constant-force measurements. The initial slope of the force-extension curve is shown in black. Representative simulation snapshots for each regime are overlaid. Pull groups, defined as the first 50 and last 50 beads, are highlighted in orange. To see this figure in color, go online.

properties of model chromosomes in a simulated stress-relaxation experiment. Chromosomes respond to force as a viscoelastic spring, with relaxation times in good agreement with experimental measurements on the order of seconds (6). Finally, we investigate how stretching alters the chromosome's internal organization. In the low-strain regime, we find that stretching perturbs large-scale chromosome organization while leaving local chromatin structure largely unaffected. Contact maps respond very differently to applied force in interphase and mitosis, suggesting distinct mechanisms of chromosome elasticity. Our work suggests that the forces underlying the spatial organization of the chromosome are also responsible for their mechanical behavior.

METHODS

Using the MiChroM energy function, we simulated DT40 chromosome 7 in both interphase and mitosis (specifically, prometaphase, i.e., 15 min after release from G2 arrest). The DT40 cell line was chosen due to the availability of high-resolution Hi-C contact maps corresponding to interphase and mitosis of the same cell line (23). Chromosome 7's small size allowed for rapid simulations. Our model chromosomes are coarse-grained polymers consisting of 739 beads at 50 kb resolution. Chromosomes are simulated using Langevin dynamics at an effective temperature, subjected to a Hamiltonian made up of three components. The homopolymer potential includes bonding between neighboring polymers, bending rigidity of the polymer chain, and excluded volume interactions. Overlap between non-nearest neighbors is permitted with a finite energy penalty, allowing for topological relaxation of the polymer through chain crossing. This captures the effect of topoisomerase type II enzymes, which cuts DNA allowing for chain crossing to remove entangled structures. The type-type potential encodes interactions that depend on the epigenetic character of the participating segments of chromatin, resulting in phase separation of chromatin into compartments. The ideal chromosome term encodes genomic-distance-dependent interactions, which lead to lengthwise compaction of the chromosome, capturing the effect of loop-extruding motors such as cohesin and condensins (30).

We use parameters for the model that best agree with the experimental Hi-C maps of chicken DT40 cells (Figs. S1 and S2). While the symbolic form of the energy landscape is the same for interphase and mitosis, the learned interaction parameters differ to reflect the Hi-C contact maps taken from interphase and mitotic cells. The learned type-type interaction parameters are much larger for the interphase model, reflecting the strong compartmentalization signal (checkerboard pattern) present in the interphase Hi-C contact map. During mitosis, the compartmentalization signal disappears and chromosomes are compacted into rod-like structures with a greater frequency of long-range interactions and a non-monotonic contact scaling curve (23). As a result, the type-type interaction parameters learned for the mitotic chromosome are much smaller and the ideal chromosome interaction parameters decay more slowly with genomic distance. Using the iterative optimization scheme described in (25) to fit the model, we achieve Pearson's correlations of 0.91 and 0.9 in interphase and mitosis, respectively. The simulations were carried out using the OpenMiChroM software package (37,38). OpenMiChroM is a Python library for performing chromatin dynamics simulations using GPU hardware acceleration through OpenMM Python API (39).

To probe the mechanical properties of these model chromosomes, we subjected them to axial stretching by applying pulling forces and orientation constraints to the centers of mass of the first 50 and last 50 beads of the polymer chain. Concretely, we write the centers of mass of the "pull groups" as follows:

$$\begin{aligned} \mathbf{R}_{left} &= (x_l, y_l, z_l) = \frac{1}{50}\sum_{i=1}^{50}\mathbf{r}_i \\ \mathbf{R}_{right} &= (x_r, y_r, z_r) = \frac{1}{50}\sum_{i=N-49}^{N}\mathbf{r}_i \end{aligned} \tag{1}$$

We define a pull coordinate $\xi = x_r - x_l$ as the chromosome's end-to-end x-distance. In chromosome-pulling experiments, the ends of the

chromosome are held by micropipettes and one is moved along a linear track. To mimic this process, we introduce orientation constraints:

$$\begin{aligned} \mathbf{U}_{pin} &= \frac{1}{2}k_r\left(x_l^2 + y_l^2 + z_l^2\right) \\ \mathbf{U}_{slide} &= \frac{1}{2}k_r\left(y_r^2 + z_r^2\right) \end{aligned} \tag{2}$$

$\mathbf{U}_{pin}$ restrains the center of mass of the left pull group to the origin. $\mathbf{U}_{slide}$ restrains the right pull group to the x axis, but allows it to slide along the x axis. A large value $k_r = 10^5\varepsilon/\sigma^2$ is used so that $\mathbf{R}_{left} \approx 0$ and $y_r, z_r \approx 0$. We use two methods to subject the simulated chromosomes to axial strain. In constant-force (CF) pulling, a linear potential is used to apply a constant elongating force to the pull coordinate ξ. In constant-distance (CD) pulling, a harmonic potential with a very strong spring constant is used to constrain ξ to a very small window around a chosen reference distance ξ_0.

$$\begin{aligned} \mathbf{U}_{CF} &= -F\xi \\ \mathbf{U}_{CD} &= \frac{1}{2}k_p(\xi - \xi_0)^2 \end{aligned} \tag{3}$$

A large value of $k_p = 10^5\varepsilon/\sigma^2$ is chosen so that $\xi \approx \xi_0$ during CD sampling. These two pulling strategies are shown schematically in Fig. 1. These potentials acting on the centroids of the pull groups are implemented using the CustomCentroidBondForce class built into OpenMM (39).

In a CF simulation, chromosomes are equilibrated under the combined action of the MiChroM potential, $\mathbf{U}_{pin}$, $\mathbf{U}_{slide}$, and $\mathbf{U}_{CF}$. $\mathbf{U}_{CF}$ acts effectively to bias the pull coordinate ξ toward larger values, but does not constrain ξ to any particular value. An ensemble of equilibrium structures are recorded. During these simulations, ξ fluctuates over a relatively large interval. The histograms in Fig. S3, *A* and *D*, show the probability distributions $p_F(\xi)$ of ξ during CF pulling at each chosen force value F. To create a force-extension curve, a single value $\xi(F)$ must be chosen for each force F. The correct choice is $\xi(F) = \text{argmax}[p_F(\xi)]$, as explained in the supporting material. In a CD simulation, chromosomes are equilibrated under the combined action of the MiChroM potential, $\mathbf{U}_{pin}$, $\mathbf{U}_{slide}$, and $\mathbf{U}_{CD}$. $\mathbf{U}_{CD}$ constrains the pull coordinate ξ to a very small window around a chosen reference distance ξ_0 by exerting a restoring force $F_{CF} = -k_p(\xi - \xi_0)$ on the pull coordinate. An ensemble of equilibrium structures are recorded, and the force is determined by averaging this restoring force over the generated ensemble:

$$F(\xi_0) = \langle -k_p(\xi - \xi_0)\rangle \tag{4}$$

This force measurement method is justified more rigorously in the supporting material and Fig. S6.

RESULTS AND DISCUSSION

Chromosomes behave as linear elastic material in the small-strain regime

We measured the force-extension behavior of our model chromosomes using both the CF and CD pulling methods (see methods). The resulting force-extension curves are shown in Fig. 1, *C* and *D*. When subjected to low extensile axial force, model chromosomes behave like a linear elastic material. This means chromosome strain, defined as the ratio of the increase in the end-to-end extension to the native contour length, is linearly proportional to the applied axial force. The spring constant associated with the weak stretching of the chromosomes is obtained from the slope of the force-extension curve, with dimensions of force per unit length. We obtained spring constants of $k = 0.09\varepsilon/\sigma^2$ and $k = 0.73\varepsilon/\sigma^2$, respectively, for models of interphase and mitotic chromosomes, suggesting a near 10-fold stiffening of chromosomes in mitosis. Linearity of force-extension curves (Hooke's law) has been experimentally observed for mitotic chromosomes (5,14). Similarly, recent rheology measurements in the interphase genome have indicated a weaker mechanical response (1). The energy functions describing interphase and mitotic chromosomes are functionally identical. Parameters describing the properties of the chromatin chain (bond stiffness, bending rigidity, and excluded volume interactions) are identical across models, and the type-type and ideal chromosome potentials for interphase and mitosis diverge only in the numerical values of parameters describing the strength of compartmentalization and lengthwise compaction interactions (see Fig. S1). These parameters are learned solely from chromosome-contacts data, so that MiChroM recapitulates well the organization of interphase and mitotic chromosomes. The marked increase in stiffness from interphase to mitosis demonstrates that the chromosome's mechanical properties are heavily influenced by its large-scale organization.

The force required to stretch a mitotic chromosome to double its native length in vitro is typically in the range of $0.1 - 1$ nN (14), which can be compared with the extrapolated doubling force of $9.5\varepsilon/\sigma$ for the simulated mitotic chromosome, suggesting that the reduced unit of force $\varepsilon/\sigma \sim 10 - 10^2$ pN. In the supporting material, we calibrate the model's length scale (in mitosis) to be $\sigma = 0.096\ \mu$m by matching the densities of the simulated and experimental mitotic chromosome. The reduced energy unit ε is an information-theoretic temperature, which sets the energy scale of interactions between chromosome beads (containing hundreds of nucleosomes); in other words, the typical energy required to strain the interface between two 50 kb segments of chromatin is of the order of ε. Substituting $\sigma = 0.096\ \mu$m into the relation $\varepsilon/\sigma \sim 10 - 10^2$ pN, we find $\varepsilon \sim 10^2 - 10^3 K_BT$ (recall $K_BT = 4.11$ pN $\cdot$ nm).

Note that the CD method of pulling chromosomes provided a direct measure of the chromosome's native length (Fig. 1). Whenever the two pull groups were closer than the native length of the chromosomes there was a compressive load on the external springs holding the pull groups. Simply put, in CD ensemble, the extension corresponding to the zero force in the force-extension curve gives the chromosome's native length. We find that the native length of mitotic chromosomes is about twofold higher than that of interphase chromosomes.

Chromosomes unravel under strong axial stretching

When stretched to lengths near double their native length, model chromosomes lose their structural integrity as the polymer separates into blobs connected by a single-bead-thick

chromatin thread. In interphase, the unraveling leads to a plateau in the force-extension curve. In mitosis, there appears a sharp dip in the force-extension curve at the onset of unraveling, followed by a plateau (see Fig. 1). Chromatids assembled in vitro from *Xenopus* egg extracts have been observed to segregate into domains of thick chromatin connected by thin filaments when stretched to lengths greater than 15 times their native length (8). A blob-and-thread geometry was also observed in stretched mitotic newt chromosomes when treated with Micrococcal nuclease (an enzyme that cuts DNA) (14). For model chromosomes, this rupture can be understood as a consequence of free energy minimization. As the chromosome stretches uniformly, its surface area increases, decreasing the number of (energetically favorable) bead-to-bead contacts. When stretched past rupture, the chromosome segregates into a "dense" phase, where the chromosome contacts are preserved, and a "rare" phase characterized by a bare segment of polymer. Rupture occurs when the energetic benefit of preserving native contacts in the dense phase outweighs the entropic cost of phase separation (see Fig. S14 *E*). The sudden drop in the restoring force upon unraveling of mitotic chromosomes suggests that the transition to the coexistence of dense and rare phases is abrupt. For the interphase chromosome, the onset of phase coexistence is smooth, likely due to its lower mechanical stiffness. When pulling under constant force, the condensed state becomes metastable when the applied force exceeds a threshold. Beyond this force capacity, the chromosome will fully unravel. The behavior of interphase and mitotic chromosomes under constant forces larger than those shown in Fig. 1 is shown in Fig. S17.

Stress relaxation in simulated chromosomes is well captured by a linear viscoelastic model

We measured the dynamics of chromosome extension in a stress-relaxation simulation, and found that the chromosome response to sudden stress is well captured by a linear viscoelastic Kelvin-Voight (KV) model, which is a minimal model consisting of a linear dashpot (viscous component) with viscosity η and a linear (Hookean) spring with spring constant k attached in parallel (Fig. 2). When the KV model is subjected to an external stress F, the end-to-end extension ξ evolves in time following: $\eta\dot{\xi} = F - k(\xi - \xi_0)$. After the sudden application of stress to the chromosome, its extension ξ increases at an exponentially decaying rate: $\xi(t) = \xi_0 + (F/k)(1 - \exp(-t/\tau_r))$. The saturation extension, $\xi(t \to \infty) = \xi_0 + F/k$, controlled by the spring constant, increases linearly with the applied stress according to Hooke's law. After the pulling force is suddenly released, the chromosome's extension returns to its native length following an exponential decay: $\xi(t) = \xi_0 + (F/k)\exp(-t/\tau_r)$. Other simple models for viscoelastic behavior (e.g., the Maxwell model) display a "creep" behavior under stress or a sudden jump upon the sudden application of a stress, neither of which were observed in simulations. In Fig. 2, we fit the trajectories of the chromosome's extension to the KV model, and determine the relaxation time τ_r, which are 1.2 and 18 s, respectively, for mitosis and interphase. These relaxation times represent the timescale over which all the internal modes of fluctuations of the chromosomes relax, and the perturbed extension reaches equilibrium. Due to their higher mechanical stiffness, compact mitotic chromosomes relax faster than the less compact interphase chromosomes. The relaxation timescale of 1.2 s measured for the mitotic chromosome is in good agreement with experimentally measured values on the order of seconds (7). The relaxation timescales for stretching of a whole interphase chromosome have not, to our knowledge, been measured. Some experiments have, however, measured the relaxation timescale upon application of a force to a single genomic locus via a bound magnetic particle, finding minutes-long timescales for the relaxation (1), suggesting a longer relaxation timescale for the interphase chromosome compared with the mitotic chromosome. This trend is in agreement with our model and is a result of the higher compaction of mitotic chromosomes.

We note that the relaxation times measured in simulation are in good agreement with those estimated for a free-draining polymer. When a tension F is applied to the chromosome of spring constant k, its extension will increase by a distance of $d = F/k$. Thus, the chromosome's center of mass will change by a distance of $d_{mean} = F/2k$. If relaxation occurs with a characteristic timescale τ_r, the mean center-of-mass velocity during relaxation is approximately $v_{cm} \approx d_{mean}/\tau_r = F/(2k\tau_r)$. Chromosome 7 has $N = 739$ beads each of mass 10, and with friction constant of $\gamma = 0.1\tau^{-1}$. The net drag of the chromosome's center of mass is $\zeta = Nm\gamma$. Therefore, the total drag force on the chromosome during stretching is approximately $F_{drag} \approx \zeta v_{cm}$. Setting the drag force and applied force equal, we obtain a relaxation time estimate of $\tau_r \approx Nm\gamma/2k$. This gives estimates of $\tau_r \approx 4000\tau$ and $\tau_r \approx 500\tau$ for interphase and mitosis, respectively, in good agreement with simulated measurements (see Fig. 2 *I*) The reduced time unit τ is calibrated in the supporting material. Note that the conversion factor to real time units is larger in interphase than mitosis, due to the different length scales of the models. Experiments probing the mitotic chromosomes find a relaxation timescale of roughly 2 s (6), which is in excellent agreement with the value obtained from simulation (Fig. 2 *I*).

Stretching perturbs interphase chromosomes at the site of pulling, while mitotic chromosomes distribute stress along their axial length

Having quantified the mechanical properties of our model chromosomes, we now seek to understand the mechanisms that underlie their elasticity. To do so, we use a variety of structural analyses to observe how the chromosome's internal structure is perturbed by axial stretching. In Fig. 3, we

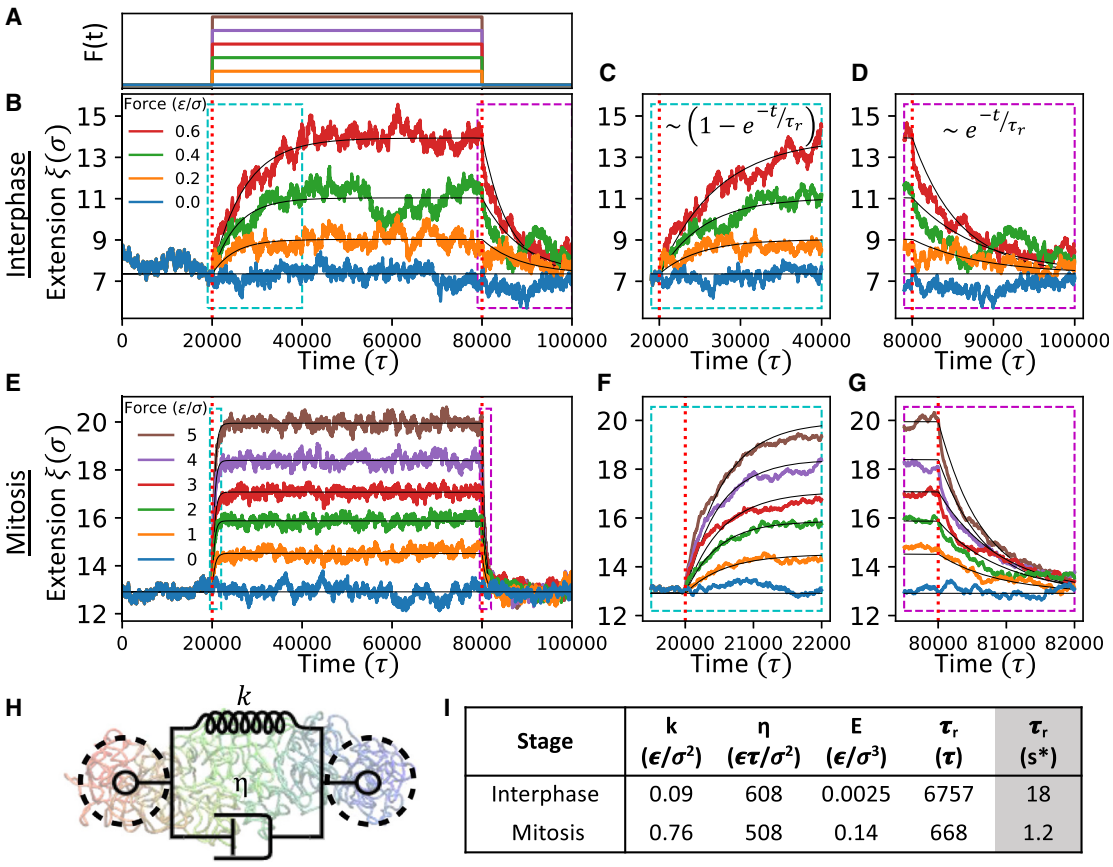

I

Stage	k (ϵ/σ^2)	η ($\epsilon\tau/\sigma^2$)	E (ϵ/σ^3)	τ_r (τ)	τ_r (s*)
Interphase	0.09	608	0.0025	6757	18
Mitosis	0.76	508	0.14	668	1.2

FIGURE 2 Viscoelastic relaxation dynamics of simulated chromosomes. (*A*) F(t) exerted on chromosomes during stress relaxation experiments. For interphase, force values are (in reduced units) $0, 0.2, 0.4$, and 0.6 ($F = 0.8$ not shown due to chromosome unraveling). For prometaphase, force values are (in reduced units) $0, 1, 2, 3, 4$, and 5. (*B* and *E*) Mean extension versus time plot during stress-relaxation experiment for interphase. Force is applied at time $20,000\tau$ and released at $80,000\tau$. Chromosome extension ξ shown is averaged over 40 replica trajectories to reduce noise. Thin black lines show fit of mean chromosome extensions to the exponential decays indicated in the expressions at the top right. (*C* and *F*) More detailed view of chromosome's response to the sudden force onset. (*D* and *G*) More detailed view of chromosome's response to the sudden force release. (*H*) Chromosome behavior is compared with that of a simple Kelvin-Voigt model with a spring constant and viscosity. (*I*) Kelvin-Voigt parameters of best fit. k is spring constant, η is viscous damping constant. The intrinsic analogs of these parameters (elastic modulus E and relaxation time τ_r) are listed as well. Quantities are expressed in reduced units. *Relaxation time is also converted to units of seconds (see supporting material). For mitotic chromosome, measured relaxation time of $1.2\ s$ matches well with experimental results. Note that the trajectories $\xi(t)$ shown are averaged over 40 replica trajectories of each model chromosome. The trajectories of individual chromosomes are compared with the mean in Fig. S5. To see this figure in color, go online.

plot Hi-C contact maps of interphase and mitotic chromosomes in the absence of applied tension, with an applied tension, and the residual difference map. In the absence of applied tension, the interphase chromosome's telomeres colocalize under the combined influence of compartmentalization interactions favoring contacts between loci of like epigenetic character and the entropic favorability of end-to-end proximity induced by their confinement to the x axis (see supporting material). When tension is applied, the telomeres move apart leading to a depletion of contact probability at the antidiagonal extremities of the contact map (Fig. 3, *A–C*). In contrast, the mitotic chromosome distributes applied tension along its length, leading to a nearly translation-invariant pattern of contact probability changes in its Hi-C contact map (Fig. 3, *E–G*). Contacts are depleted at all genomic separations except for a band around 3–5 Mb of separation where tension *increases* contact probability (see Fig. S4, *bottom right*). Stretched mitotic chromosomes have a straighter backbone (Fig. 4), which may enhance structural helicity, leading to a more prominent non-monotonic scaling of contact probability. Videos S1 and S2 show how interphase and mitotic chromosome contact maps change as chromosomes are stretched using the CD pulling method.

Compartmental interactions mediate interphase chromosome elasticity while lengthwise compaction drives mitotic chromosome elasticity

We also examined the effects of stretching on each component of the MiChroM energy functional. In Fig. 3, *D* and *H*, we plot the interphase and mitotic model's mean potential energy components as a function of the externally applied tension, relative to the zero-tension ensembles. Pulling interphase

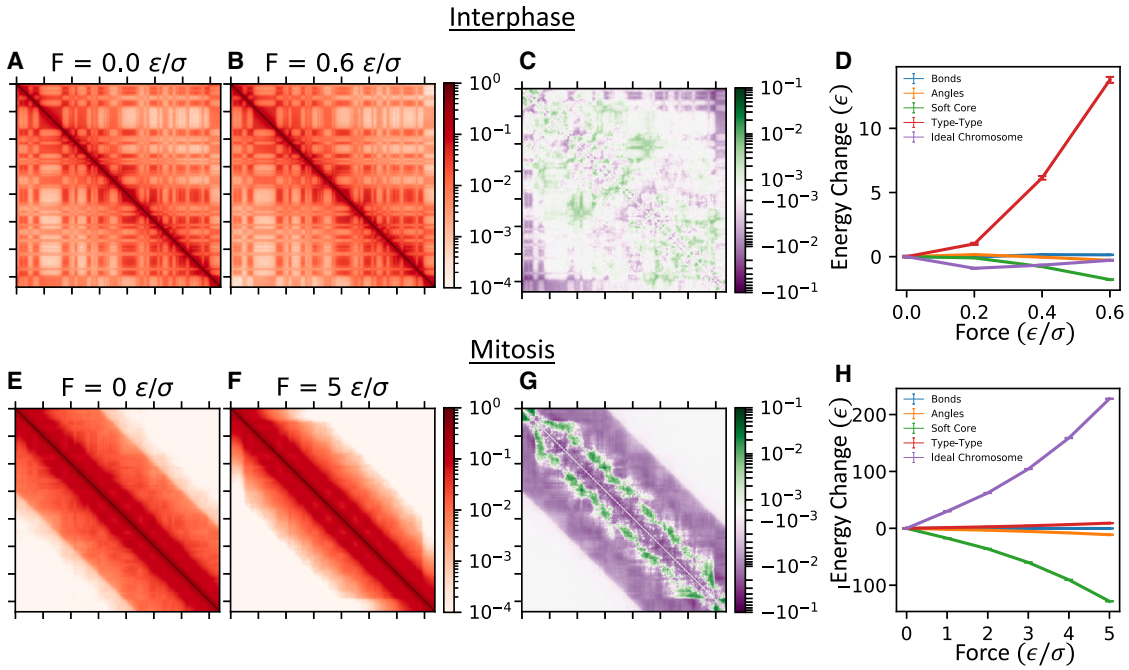

FIGURE 3 Perturbations to chromosome's contact map and potential energy components under tension for interphase (*top*) and mitosis (*bottom*). (*A* and *E*) Simulated Hi-C contact maps of the interphase/mitotic chromosome under CF setup with applied force 0. (*B* and *F*) Simulated Hi-C contact maps of the interphase/mitotic chromosome under CF setup with applied force $0.6\frac{\epsilon}{\sigma}/5\frac{\epsilon}{\sigma}$. (*C* and *G*) The difference between the contact maps for chromosomes under tension (*B* and *F*) and not under tension (*A* and *E*). Contact probability plotted on a symmetric log scale with linear cutoff 10^{-3}. (*D* and *H*) Mean potential energy components of the interphase/mitotic chromosome under tension. Bonds, angles, and soft-core potential energy components are included in the homopolymer potential. In interphase, pulling primarily disrupts type-type interactions that depend on the epigenetic types of interacting loci. In mitosis, pulling primarily disrupts ideal-chromosome interactions that depend on the genomic distance between loci. Note that the decrease in the average soft-core potential arises due to the depletion of contacts and the increased self-avoidance during pulling. This decrease in the soft-core potential with increasing force is more apparent in the mitotic chromosome, due to its more compact state compared with the interphase chromosome. Vertical error bars show standard error of the mean over 40 replica trajectories. To see this figure in color, go online.

chromosomes results mainly in an increase in the type-type potential energy component, whereas pulling mitotic chromosomes results mainly in an increase in the ideal chromosome component. This suggests that distinct mechanisms underlie the elasticity of interphase and mitotic chromosomes: interphase chromosome elasticity arises from mechanical rigidity of chromatin compartments while mitotic chromosome elasticity arises from SMC-driven lengthwise compaction. To control for the overall scale of the type-type and ideal chromosome potential energy components, we also plot the fractional change in these potentials under force (Fig. S18). We find that stretching perturbs type-type interactions in both interphase and mitosis—type-type interactions contribute less to the mechanical response in mitosis because the type-type interaction parameters are much weaker in the mitotic chromosome. However, stretching perturbs lengthwise compaction (ideal chromosome) interactions only in mitosis.

Chromosomes undergo large-scale rearrangements under tension

We seek to understand how the different spatial scales of the interphase and mitotic chromosome participate in chromosome stretching. To that end, we perform a renormalization-based analysis of the simulated trajectories. To "view" simulated chromosome structures at an arbitrary length scale of w beads, we average the positions of the polymer beads in the full structure over a sliding window of w beads. The resulting "renormalized" chain at scales $w = 20$ beads (1000 kb) and $w = 100$ beads (5000 kb) are visualized in Fig. 4. To understand the effect of stretching on the chromosome at various scales, we may observe the effect of stretching on these coarse-grained representations of the full chromosome at various scales w.

We analyzed the bond correlation function at different coarse-graining lengths: $\tilde{T}^{w}(\Delta)$ (Fig. 4). This quantity, bound between -1 and 1, is the mean cosine of the angle made by a pair of bonds that are Δ distance apart along the contour. Values close to zero indicate that the directions of bonds are uncorrelated. Positive/negative values indicate that bonds tend to be aligned/antialigned. An increase in the tangent-tangent correlation function indicates a "straightening" of the chromosome at the renormalization scale w. We expect a decay for neighbors because of the stiffness of the polymer, while the non-monotonic behavior after the initial decay is due to looping back of the chromosome. Note that the non-monotonic oscillations depict a

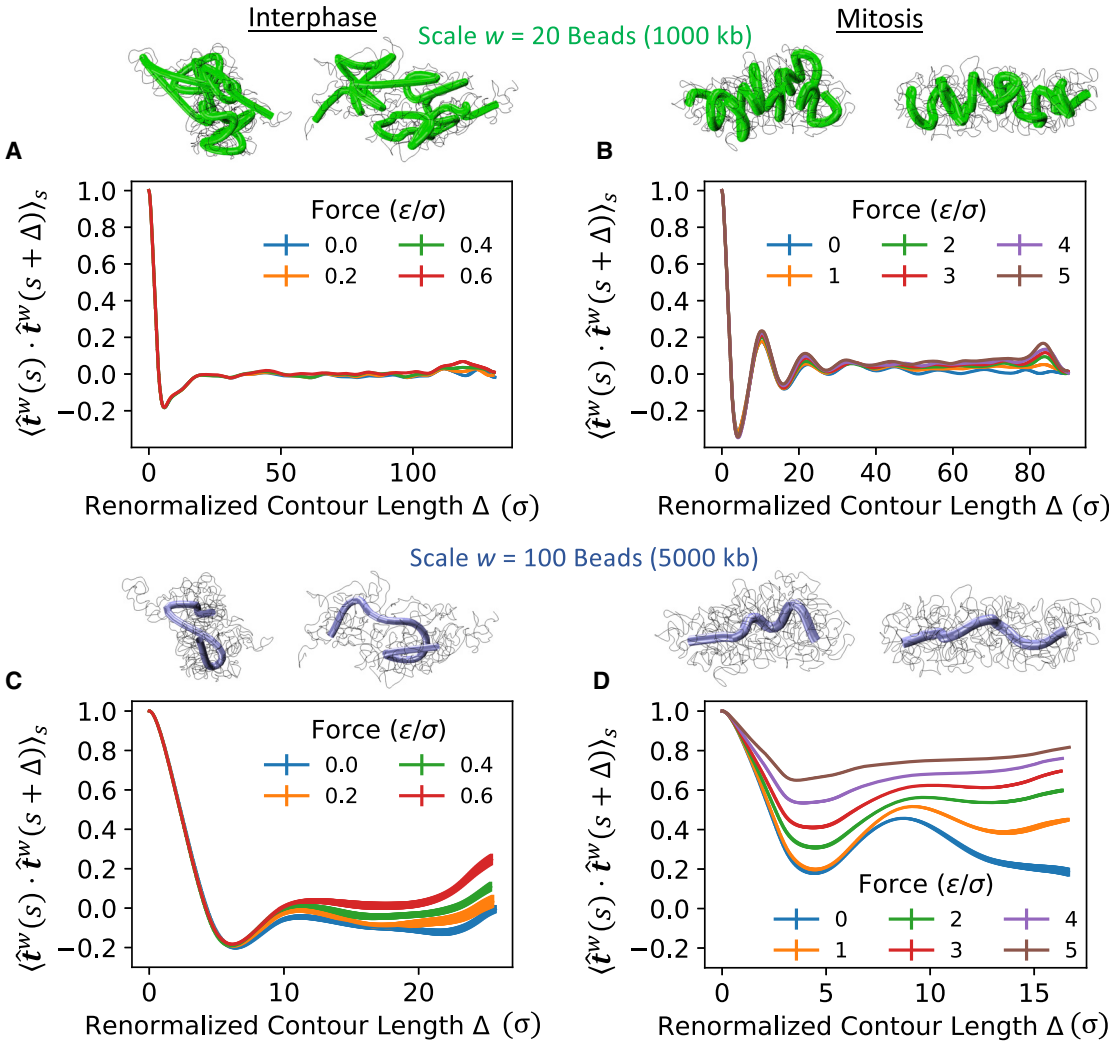

FIGURE 4 Pulling causes reorganization of large-scale chromosome architecture. (*A* and *C*) Effect of tension on the interphase chromosome renormalized at the scale of $w = 20/w = 100$ beads (1000 kb/5000 kb). Above plots, representative simulation snapshots are shown under force $F = 0$ (*left*) and $F = .8\frac{\varepsilon}{\sigma}$ (*right*). Full chain is shown as a thin black line with renormalized chain $\tilde{r}_i^w$ shown as a tube. Plots show renormalized tangent correlation functions $\tilde{T}^w(\Delta) = \langle \hat{\mathbf{t}}^{\mathbf{w}}(s) \cdot \hat{\mathbf{t}}^{\mathbf{w}}(s+\Delta) \rangle_s$ for chromosomes under constant force $F = 0, 0.2, 0.4, 0.6$. (*B* and *D*) Effect of tension on the mitotic chromosome renormalized at the scale of $w = 20/w = 100$ beads (1000 kb/5000 kb). Above plots, representative simulation snapshots are shown under force $F = 0$ (*left*) and $F = 5\frac{\varepsilon}{\sigma}$ (*right*). Full chain is shown as a thin black line with renormalized chain $\tilde{r}_i^w$ shown as a tube. Plots show renormalized tangent correlation functions $\tilde{T}^w(\Delta) = \langle \hat{\mathbf{t}}^{\mathbf{w}}(s) \cdot \hat{\mathbf{t}}^{\mathbf{w}}(s+\Delta) \rangle_s$ for chromosomes under constant force $F = 0, 1, 2, 3, 4,$ and 5. Vertical error bars show standard error of the mean over 40 replica trajectories. To see this figure in color, go online.

long-range helical order along the chromosome backbone, which is enhanced in mitosis. With increasing stretching force, the bonds align along the external force, but the reorientation is significant only at length scales above 100 beads (~5 Mb) in interphase and 50 beads (~ 2.5 Mb) in mitosis, suggesting significant perturbation of the structure only at these large length scales. Our analyses of the linear compaction along the renormalized chain $C(w)$, defined as the ratio of contour length of the full polymer to the contour length of the renormalized chain at scale w, and the radius of gyration of the renormalized window, are consistent with the 100/50 bead (~5/2.5 Mb) length scale as a characteristic length for structural perturbation under small strain in interphase/mitosis (see supporting material and Figs. S7–S13).

Mitotic chromosomes behave as stiff elastic rods

Bending rigidity and persistence lengths are two important coefficients that characterize the mechanical response of chromosomes (5,8,14). We measured the persistence length (L_p) and bending rigidity (B) of our model mitotic chromosomes (recall, $B = K_B T L_p$ (40)). To allow for accurate measurement of persistence length, we extended the length of the chromosome by joining 10 copies in series (and allowing for type-type and ideal chromosome interactions between

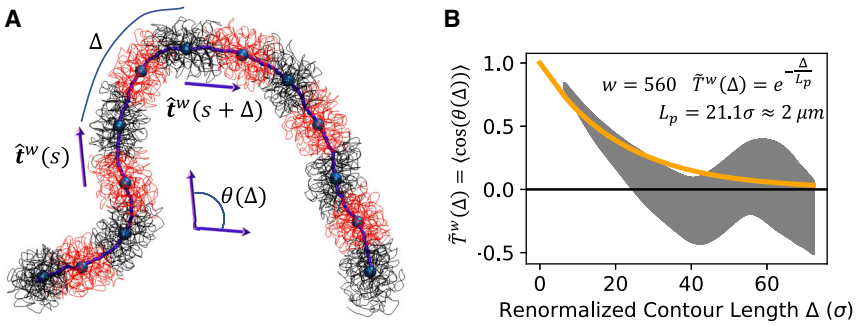

FIGURE 5 Bending rigidity of the prometaphase chromosome. (*A*) Simulation snapshot of 7390-bead mitotic chromosome. Renormalized chain $\tilde{\mathbf{r}}_i^{\mathbf{w}} = \frac{1}{w}\sum_{l=i}^{l+w-1}\mathbf{r}_l$ for $l \in \{1, 2, \ldots, N-w+1\}$ is shown in purple. One set of nearest non-overlapping neighbor renormalized beads $\{\tilde{\mathbf{r}}_1^{\mathbf{w}}, \tilde{\mathbf{r}}_{1+w}^{\mathbf{w}}, \tilde{\mathbf{r}}_{1+2w}^{\mathbf{w}}, \ldots\}$ is shown as large blue spheres. Blue spheres are the centers of mass of the associated chromatin windows shown in alternating red and black thin tubing. A natural scale of $w = 560$ beads is chosen self-consistently so that chromosome radius equals mean renormalized bond length (the distance between *blue spheres*, see Fig. S15 for details). Purple arrows represent renormalized bonds used to calculate the renormalized tangent correlation function. (*B*) Renormalized tangent correlation function of the mitotic chromosome's thin core (see supporting material). Gray region shows standard error of the mean over four replica trajectories. Correlation function is fit to a decaying exponential to determine persistence length. To see this figure in color, go online.

concatenated chromosomes, effectively creating a single elongated chromosome). Note that, as persistence length is an intensive property, increasing the chromosome's length will not affect the persistence length. The persistence length of chromosomes that are reported experimentally is related to the bending persistence of the chromosome axial backbone. Hence, we calculated the core or backbone of the mitotic chromosome by averaging the bead positions over a sliding window of $w = 560$ beads. This window size was chosen so that the diameter of the chromosome equals the mean renormalized bond length (see supporting material and Fig. S15 for details). We then calculate the persistence length by fitting the bond vector correlations obtained at the coarse-graining length scale of $w = 560$ to the following equation: $\tilde{T}^{560}(\Delta) = \exp(-\Delta/L_p)$.

Our analysis reports the persistence length associated with backbone bending of the mitotic chromosome to be $(L_p)_{measured} = 21.1\sigma \approx 2.0\ \mu$m (Fig. 5 *B*). This is in excellent agreement with the expected persistence length of a linear material with given radius $(r = 3.24\sigma)$ and force constant $(f_0 = 9.5\varepsilon/\sigma)$: $(L_p)_{expected} = f_0 r^2/(4K_B T) = 25\sigma \approx 2.4\ \mu$m. This suggests that, as the mitotic chromosome bends, stress is distributed homogeneously over its cross section. Experimental measurements reached the same conclusion for mitotic chromosomes extracted from newt and *Xenopus* cells (14,41). The persistence length of DT40 mitotic chromosomes has not been measured, but a persistence length of 2F μm appears visually consistent with images of mitotic chromosomes 15 m after release from G2 arrest (see Fig. 1 in (23)). The obtained persistence length of 21.1σ is approximately 3.3 times the diameter of the mitotic chromosome. This is much smaller than the ratio measured for mitotic chromosomes extracted from Newt and *Xenopus* cells (14,41), but matches well the experimentally measured ratio of 3.4 for chromatids assembled from *Xenopus* egg extracts (8). Zhang and Heermann use a similar strategy to measure the persistence length of another model for the mitotic chromosome, similarly finding persistence lengths from 1.5 to 4 times the diameter of their model chromosomes (42). Metaphase chromosomes retrieved from living *Xenopus* or newt cells had much larger persistence lengths ranging from millimeters to centimeters (7). The lower values of persistence length in our prometaphase model may also be attributed to partially condensed chromosomes in prometaphase compared with metaphase.

DISCUSSION

In this work, we have tested the mechanical properties of a bead-spring polymer model of chromosomes with data-driven force fields (25) by subjecting it to external stretching, mimicking tweezers-style experiments (5,14). The data-driven force field comprises three components: first, the homopolymer potential contains terms such as the nearest neighbor bonds and intermonomer self-avoidance; second, the phase separation potential that drives compartmental segregation; and third, lengthwise compaction, encoded by the ideal chromosome potential, that crumples the polymer resembling the steady-state loop-extrusion activity of SMC complexes (30). Note that the prometaphase chromosomes of chicken DT40 cells show a non-monotonic trend in the scaling of contact probability with genomic distance, suggesting an increase in contact frequency between genomic segments that are ~ 4 Mb apart (23). We find that using a non-monotonic ideal chromosome potential is necessary to recapitulate the high intensity stripe pattern running parallel to the diagonal (see Fig. S1).

We pull the chromosomes using two different techniques (CF and CD), and show that our results are consistent (Fig. 1). Both interphase and mitotic chromosomes show a linear force-extension curve in the small-strain regime, behaving like a linear elastic material. However, mitotic chromosomes are about 10-fold stiffer than the interphase ones under stretching perturbations (Fig. 1). The native contour length, i.e., the end-to-end distance for zero stretching force, of mitotic chromosomes is about twofold higher than

interphase chromosomes. Matching the mitotic chromosome's extrapolated doubling force measured in simulations to the typical doubling force observed in experiments, we back-solve to estimate the reduced energy unit, finding $\varepsilon \sim 10^2 - 10^3 K_B T$. This value sets the energy scale for interactions between beads representing 50 kb of chromatin. The density of cross-linking proteins in mitotic chromosomes has been estimated as approximately 1 connector protein every 6 kb of chromatin (5,43). Thus, we expect the pairwise interactions between beads in MiChroM to capture the action of approximately 10 cross-linking proteins. An estimate of $\varepsilon \sim 10^2 - 10^3 K_B T$ is reasonable in this context.

When stretched to more than twice their native contour length (i.e., larger than 100% strain), the chromosomes begin to unravel into a blob-and-thread structure. The unraveling force for mitotic chromosomes is about 10-fold higher than interphase. Similar unraveling has been observed in experiments, although at very high strains (5,14). Mechanical perturbations of interphase chromosomes are much less explored experimentally; nonetheless, initial studies indeed suggest a mechanical rigidity that is much weaker than mitotic chromosomes (1).

When subjected to a sudden stress, model chromosomes show slow relaxation just like a viscoelastic material (Fig. 2). Using a linear viscoelastic KV model, we were able to extract relaxation times corresponding to interphase ($\sim$ 20 s) and mitotic ($\sim$ 2 s) chromosomes (Fig. 2). The faster relaxation of mitotic chromosomes may be attributed to their higher mechanical stiffness that leads to a faster decay of the fluctuation modes. The extracted relaxation times for mitotic chromosomes are in good quantitative agreement with experimental findings (14).

Stretching perturbs the structure of interphase and mitotic chromosomes in qualitatively distinct ways. While the weak restoring force upon stretching interphase chromosomes arises from disrupting compartments and separating the telomeres; the stiff response from stretching mitotic chromosomes comes from SMC-driven lengthwise compaction (Fig. 3). Interestingly, our model predicts that the stripe pattern in the mitotic Hi-C map is enhanced upon stretching (Fig. 3). The stripe, controlled to condensin II activity (23), signifies emergence of helical order along the backbone of the chromosomes. When there is no stretching force, the entropy of the backbone obscures its helical order; however, as the entropic excursions of the backbone are suppressed by external force, the signature corresponding to the helical order becomes stronger. This is a direct prediction of our model and remains to be experimentally validated.

Force-induced structural rearrangements in our model occur at length scales near 100 beads or 5 Mb (Fig. 4). This suggests that the source of linear elasticity in our model comes from rearrangements of large chunks of DNA that maintain their internal hierarchical organization, but displace relative to each other. We also measured the bending rigidity and persistence length of our model prometaphase chromosomes (Fig. 5). The measured values are consistent with the theoretical expectation from a linear elastic rod of the structure; however, experimental observations for chicken DT40 prometaphase chromosomes are lacking at the moment.

The reversible linear elasticity of mitotic chromosomes appears to span a wider strain regime in experiments (5) than our model. This may arise from the fact that MiChroM is trained to reproduce *population-averaged* Hi-C contact maps, so that mechanically robust contacts in single cells are averaged into weaker population-wide spatial associations. MiChroM treats all cell-cell variability in chromosome structure as *annealed* disorder. While we simulate many copies of a chromosome in parallel to speed sampling, in principle the population-averaged contact map could be recovered as the long-time average contact map of a single chromosome. The extent to which individual chromosomes explore the space of folded conformations in vivo is at present unclear. Single-cell interphase Hi-C contact maps have demonstrated large variability in chromosome structure between cells of the same population, and have much sparser contact maps than population-averaged Hi-C (44). In addition to annealed disorder, cell-cell variability in epigenetic markings or random placement of stably binding cross-linkers may create *quenched* disorder between cells of the same population. If trained on these sparse single-cell Hi-C contact maps, an energy landscape model might learn a comparatively sparse set of strong interactions that resemble stable cross-linkers. Future work may investigate the mechanical properties of energy landscape models trained on single-cell Hi-C data in this manner.

The force-extension curves we obtain for the interphase and mitotic chromosome may also be compared with those of individual chromatin fibers (nucleosome-bound DNA) (45). At high salt concentration, the chromatin fiber's force-extension curve consists of a linear regime at low strain followed by a plateau, then an additional stiffening as the fiber reaches its maximum length (before nucleosomes are ejected). This behavior could be explained by a two-state model, where the chromatin fiber is considered as a worm-like chain that may locally transition between a compacted and an open state—a transition attributed to attractive interactions between bound nucleosomes. Our model similarly consists of a worm-like chain with additional attractive interactions between beads that lead to further compaction. We similarly observe a linear force-extension behavior at low strain followed by a plateau. However, this plateau is not immediately followed by a stiffening due to the chromosome's high degree of linear compaction, which leaves much more to be unraveled.

Our simulations should be compared with the simulations of Zhang and Heermann (42), who developed a "dynamic loop model" for mitotic chromosomes. This model consists of a polymer chain on a lattice. When two loci come into close spatial proximity, a cross-linking interaction can

form between them if they are separated by a contour length less than a chosen cutoff. This leads to cylindrical structures resembling mitotic chromosomes. Cross-linking interactions have a finite lifetime, and thus effectively resemble the transient interactions created by the ideal chromosome potential in MiChroM. Similarly to MiChroM, these model chromosomes display linear force-extension behavior at small strain, but unravel when strained past three times their native length, opening into a blob-and-thread geometry. The stretch elasticity of dynamic loop chromosomes depended sensitively on the concentration of cross-linkers. Also like the MiChroM mitotic chromosome, dynamic loop chromosomes have a persistence length that is only a few times their diameter.

Experiments have demonstrated that condensin compacts chromatin by actively extruding loops, deliberately bringing together loop anchors much more quickly than passive diffusion (46). However, both MiChroM (25) and the dynamic loop model (42) rely on passive diffusion to bring loop anchors into close spatial proximity. Chromosome models that include active extrusion have been implemented to explain TAD formation in interphase (47,48) and the compaction and separation of sister chromatids during mitosis (49). The mechanical properties of this class of models remain unexplored.

CONCLUSIONS

In our simulations, interphase and mitotic chromosomes are both modeled as bead-spring polymers with additional pairwise short-range interactions tuned to recreate Hi-C contact maps. We find that interphase and mitotic chromosomes respond to stretching through distinct mechanisms, as elucidated through the inferred interaction parameters of the MiChroM model for the respective interphase and mitotic Hi-C maps. The interphase chromosome responds to pulling mainly at the site of stretching, as the compartments formed by the telomeres are torn apart. The mitotic chromosome, by contrast, stretches through the depletion of both genomically distant and genomically adjacent contacts throughout its length, while contacts around 4000 kb remain intact. Up to nearly 2× extension, large-scale rearrangements allow the mitotic chromosome to stretch its end-to-end distance without losing its structural integrity.

The Minimal Chromatin Model is inferred from Hi-C contact maps, and trained only to generate an ensemble of structures consistent with experimentally measured structures. A priori, there is little reason to expect that MiChroM structures that satisfy contact patterns also properly describe the chromosome's mechanical properties. Yet, MiChroM mitotic chromosomes recapitulate many nontrivial mechanical properties of mitotic chromosomes: they reproduce the shape of the mitotic chromosome's force-extension curve for nearly twofold extensions, display slow viscoelastic relaxation dynamics, and have stretch and bending moduli related as those of an ideal elastic rod.

Stretched chromosome structures differ from native structures through rearrangements in large-scale chromosome architecture. The qualitative agreement between theory and experiment in the low-extension regime raises the possibility that mitotic chromosomes stretch through large-scale rearrangements of chromosome architecture in vivo. Indeed, spindle-generated forces are known to stretch mitotic chromosomes to only double their native length in large animal and insect cells (9), a regime well captured by MiChroM.

Other interesting observations can be gleaned by comparing our results for interphase and prometaphase chromosomes: we observe a 50-fold increase in the chromosome's elastic modulus upon condensation from interphase to mitosis, and the interphase and prometaphase force-extension curves have distinct shapes. These differences illuminate a connection between chromosome organization and chromosome micromechanics: the mechanisms that drive chromosome organization at the microscale are disrupted during chromosome stretching, leading to an elastic response. As interphase chromosomes are primarily organized through type-type compartmentalization and mitotic chromosomes are primarily organized through SMC-driven lengthwise compaction, their responses to pulling forces vary drastically. In particular, the "bump" in the mitotic chromosome's contact scaling curve at around 4000 kb creates an anchor of enhanced interactions, which maintain the mitotic chromosome's structural integrity during stretching.

In all, we studied the varied mechanical response of chromosomes as they are organized into interphase- or mitosis-specific structures. We quantify the emergent stiffness in mitotic chromosomes, and attribute it to the SMC-driven lengthwise compaction. We also found that chromosomes behave as viscoelastic solids, as captured by a KV model, where the interphase chromosomes are more liquid-like or viscous than their mitotic counterparts. Our study quantifies the mechanical aspects of the MiChroM model that will help guide future modeling efforts. Furthermore, our estimates for forces and timescales underlying features such as compartments are important for a nuanced understanding of the in vivo mechanics of chromosomes.

SUPPORTING MATERIAL

Supporting material can be found online at https://doi.org/10.1016/j.bpj.2023.03.029.

AUTHOR CONTRIBUTIONS

B.S.R. designed research, performed all simulations, designed analysis, analyzed data, and wrote the paper. S.B. designed research, designed analysis, and wrote the paper. V.G.C. implemented and trained the computational model and edited the paper. R.R.C. designed research, designed analysis, and wrote the paper. A.B.O.J. implemented the computational

model. M.D.P. designed research and edited the paper. J.N.O designed research.

ACKNOWLEDGMENTS

This work was supported by the Center for Theoretical Biological Physics sponsored by the National Science Foundation (NSF) (grants PHY-2019745 and PHY-2210291) and by the Welch Foundation (grant C-1792). J.N.O. is a Cancer Prevention and Research Institute of Texas (CPRIT) Scholar in Cancer Research. A.B.O.J. acknowledges the Robert A. Welch Postdoctoral Fellow program. BSR was supported in part by the Rice University Department of Physics and Astronomy's Summer Undergraduate Research Fellowship, as well as the Rice University Center for Theoretical Biological Physics' Opportunities for Research in Biophysics, Informatics, and Theoretical Science (ORBITS) summer program. B.S.R. was also supported by the National Institutes of Health Molecular Biophysics Training Grant NIH/NIGMS T32 GM008313. M.D.P. is supported by the NIGMS of the National Institutes of Health under award number R35GM146852. The content is solely the responsibility of the authors and does not necessarily represent the official views of the National Institutes of Health. B.S.R. thanks David Greenblott for thoughtful discussion.

DECLARATION OF INTERESTS

The authors declare no competing interests.

REFERENCES

1. Keizer, V. I. P., S. Grosse-Holz, …, A. Coulon. 2021. Live-cell micromanipulation of a genomic locus reveals interphase chromatin mechanics. Preprint at bioRxiv. https://doi.org/10.1101/2021.04.20.439763.
2. Strickfaden, H., T. O. Tolsma, …, M. J. Hendzel. 2020. Condensed chromatin behaves like a solid on the Mesoscale InVitro and in living cells. *Cell.* 183:1772–1784.e13. https://doi.org/10.1016/j.cell.2020.11.027.
3. Shimamoto, Y., S. Tamura, …, K. Maeshima. 2017. Nucleosome–nucleosome interactions via histone tails and linker DNA regulate nuclear rigidity. *Mol. Biol. Cell.* 28:1580–1589. https://doi.org/10.1091/mbc.e16-11-0783.
4. Stephens, A. D., P. Z. Liu, …, J. F. Marko. 2019. Physicochemical mechanotransduction alters nuclear shape and mechanics via heterochromatin formation. *Mol. Biol. Cell.* 30:2320–2330. https://doi.org/10.1091/mbc.E19-05-0286.
5. Poirier, M., S. Eroglu, …, J. F. Marko. 2000. Reversible and irreversible unfolding of mitotic newt chromosomes by applied force. *Mol. Biol. Cell.* 11:269–276. https://doi.org/10.1091/mbc.11.1.269.
6. Poirier, M. G., A. Nemani, …, J. F. Marko. 2001. Probing chromosome structure with dynamic force relaxation. *Phys. Rev. Lett.* 86:360–363. https://doi.org/10.1103/physrevlett.86.360.
7. Poirier, M. G., and J. F. Marko. 2002. Mitotic chromosomes are chromatin networks without a mechanically contiguous protein scaffold. *Proc. Natl. Acad. Sci. USA.* 99:15393–15397. https://doi.org/10.1073/pnas.232442599.
8. Houchmandzadeh, B., and S. Dimitrov. 1999. Elasticity measurements show the existence of thin rigid cores inside mitotic chromosomes. *J. Cell Biol.* 145:215–223. https://doi.org/10.1083/jcb.145.2.215.
9. Nicklas, R. B. 1983. Measurements of the force produced by the mitotic spindle in anaphase. *J. Cell Biol.* 97:542–548. https://doi.org/10.1083/jcb.97.2.542.
10. Meijering, A. E. C., K. Sarlós, …, G. J. L. Wuite. 2022. Nonlinear mechanics of human mitotic chromosomes. *Nature.* 605:545–550. https://doi.org/10.1038/s41586-022-04666-5.
11. Pope, L. H., C. Xiong, and J. F. Marko. 2006. Proteolysis of mitotic chromosomes induces gradual and anisotropic decondensation correlated with a reduction of elastic modulus and structural sensitivity to rarely cutting restriction enzymes. *Mol. Biol. Cell.* 17:104–113. https://doi.org/10.1091/mbc.e05-04-0321.
12. Sun, M., R. Biggs, …, J. F. Marko. 2018. Condensin controls mitotic chromosome stiffness and stability without forming a structurally contiguous scaffold. *Chromosome Res.* 26:277–295. https://doi.org/10.1007/s10577-018-9584-1.
13. Wang, J., C. Hu, …, Z. Shao. 2022. Single-molecule micromanipulation and super-resolution imaging resolve nanodomains underlying chromatin folding in mitotic chromosomes. *ACS Nano.* 16:8030–8039. https://doi.org/10.1021/acsnano.2c01025.
14. Marko, J. F. 2008. Micromechanical studies of mitotic chromosomes. *Chromosome Res.* 16:469–497. https://doi.org/10.1007/s10577-008-1233-7.
15. Lieberman-Aiden, E., N. L. van Berkum, …, J. Dekker. 2009. Comprehensive mapping of long-range interactions reveals folding principles of the human genome. *Science.* 326:289–293. https://doi.org/10.1126/science.1181369.
16. Dekker, J., K. Rippe, …, N. Kleckner. 2002. Capturing chromosome conformation. *Science.* 295:1306–1311. https://doi.org/10.1126/science.1067799.
17. Rao, S. S. P., M. H. Huntley, …, E. L. Aiden. 2014. A 3D map of the human genome at kilobase resolution reveals principles of chromatin looping. *Cell.* 159:1665–1680. https://doi.org/10.1016/j.cell.2014.11.021.
18. Beagrie, R. A., A. Scialdone, …, A. Pombo. 2017. Complex multi-enhancer contacts captured by genome architecture mapping. *Nature.* 543:519–524.
19. Quinodoz, S. A., N. Ollikainen, …, M. Guttman. 2018. Higher-order inter-chromosomal hubs shape 3D genome organization in the nucleus. *Cell.* 174:744–757.e24.
20. Olivares-Chauvet, P., Z. Mukamel, …, A. Tanay. 2016. Capturing pairwise and multi-way chromosomal conformations using chromosomal walks. *Nature.* 540:296–300.
21. Hoencamp, C., O. Dudchenko, …, B. D. Rowland. 2021. 3D genomics across the tree of life reveals condensin II as a determinant of architecture type. *Science.* 372:984–989. https://doi.org/10.1126/science.abe2218.
22. Dixon, J. R., I. Jung, …, B. Ren. 2015. Chromatin architecture reorganization during stem cell differentiation. *Nature.* 518:331–336. https://doi.org/10.1038/nature14222.
23. Gibcus, J. H., K. Samejima, …, J. Dekker. 2018. A pathway for mitotic chromosome formation. *Science.* 359:eaao6135. https://doi.org/10.1126/science.aao6135.
24. Naumova, N., M. Imakaev, …, J. Dekker. 2013. Organization of the mitotic chromosome. *Science.* 342:948–953. https://doi.org/10.1126/science.1236083.
25. Di Pierro, M., B. Zhang, …, J. N. Onuchic. 2016. Transferable model for chromosome architecture. *Proc. Natl. Acad. Sci. USA.* 113:12168–12173. https://doi.org/10.1073/pnas.1613607113.
26. Zhang, B., and P. G. Wolynes. 2015. Topology, structures, and energy landscapes of human chromosomes. *Proc. Natl. Acad. Sci. USA.* 112:6062–6067.
27. Zhang, B., and P. G. Wolynes. 2016. Shape transitions and chiral symmetry breaking in the energy landscape of the mitotic chromosome. *Phys. Rev. Lett.* 116:248101.
28. Zhang, B., and P. G. Wolynes. 2017. Genomic energy landscapes. *Biophys. J.* 112:427–433.
29. Contessoto, V. G., O. Dudchenko, …, M. Di Pierro. 2023. Interphase chromosomes of the Aedes aegypti Mosquito are liquid crystalline and can sense mechanical cues. *Nat. Commun.* 14:326. https://doi.org/10.1038/s41467-023-35909-2.
30. Brahmachari, S., V. G. Contessoto, …, J. N. Onuchic. 2022. Shaping the genome via lengthwise compaction, phase separation, and lamina

adhesion. *Nucleic Acids Res.* 50:4258–4271. https://doi.org/10.1093/nar/gkac231.eprint.

31. Contessoto, V. G., R. R. Cheng, and J. N. Onuchic. 2022. Uncovering the statistical physics of 3D chromosomal organization using data-driven modeling. *Curr. Opin. Struct. Biol.* 75:102418. https://doi.org/10.1016/j.sbi.2022.102418.
32. Di Pierro, M., R. R. Cheng, …, J. N. Onuchic. 2017. De novo prediction of human chromosome structures: epigenetic marking patterns encode genome architecture. *Proc. Natl. Acad. Sci. USA.* 114:12126–12131. https://doi.org/10.1073/pnas.1714980114.
33. Di Pierro, M., D. A. Potoyan, …, J. N. Onuchic. 2018. Anomalous diffusion, spatial coherence, and viscoelasticity from the energy landscape of human chromosomes. *Proc. Natl. Acad. Sci. USA.* 115:7753–7758. https://doi.org/10.1073/pnas.1806297115.
34. Cheng, R. R., V. G. Contessoto, …, J. N. Onuchic. 2020. Exploring chromosomal structural heterogeneity across multiple cell lines. *Elife.* 9:e60312. https://doi.org/10.7554/eLife.60312.
35. Contessoto, V. G., R. R. Cheng, …, J. N. Onuchic. 2021. The Nucleome Data Bank: web-based resources to simulate and analyze the threedimensional genome. *Nucleic Acids Res.* 49:D172–D182.
36. Bintu, B., L. J. Mateo, …, X. Zhuang. 2018. Super-resolution chromatin tracing reveals domains and cooperative interactions in single cells. *Science.* 362:eaau1783.
37. Oliveira Junior, A. B., V. G. Contessoto, …, J. N. Onuchic. 2021. A scalable computational approach for simulating complexes of multiple chromosomes. *J. Mol. Biol.* 433:166700. https://doi.org/10.1016/j.jmb.2020.10.034.
38. Oliveira Junior, A. B., C. P. Estrada, …, J. N. Onuchic. 2021. Chromosome modeling on downsampled Hi-C maps enhances the compartmentalization signal. *J. Phys. Chem. B.* 125:8757–8767.
39. Eastman, P., J. Swails, …, R. P. Wiewiora. 2017. OpenMM 7: rapid development of high performance algorithms for molecular dynamics. *PLoS Comput. Biol.* 13:e1005659. https://doi.org/10.1371/journal.pcbi.1005659.
40. Landau, L. D., E. M. Lifshitz, R. J. Atkin, and N. Fox. 2020. The theory of elasticity. *In* Physics of Continuous Media CRC Press, pp. 167–178.
41. Poirier, M. G., S. Eroglu, and J. F. Marko. 2002. The bending rigidity of mitotic chromosomes. *Mol. Biol. Cell.* 13:2170–2179. https://doi.org/10.1091/mbc.01-08- 0401.
42. Zhang, Y., and DieterW. 2011. Heermann. "Loops determine the mechanical properties of mitotic chromosomes". *PLoS One.* 6:e29225. https://doi.org/10.1371/journal.pone.0029225.
43. Belaghzal, H., T. Borrman, …, J. Dekker. 2021. Liquid chromatin Hi-C characterizes compartment-dependent chromatin interaction dynamics. *Nat. Genet.* 53:367–378. https://doi.org/10.1038/s41588-021-00784-4.
44. Nagano, T., Y. Lubling, …, P. Fraser. 2013. Single-cell Hi-C reveals cellto- cell variability in chromosome structure. *Nature.* 502:59–64. https://doi.org/10.1038/nature12593.
45. Cui, Y., and C. Bustamante. 2000. Pulling a single chromatin fiber reveals the forces that maintain its higher-order structure. *Proc. Natl. Acad. Sci. USA.* 97:127–132. https://doi.org/10.1073/pnas.97.1.127.
46. Ganji, M., I. A. Shaltiel, …, C. Dekker. 2018. Real-time imaging of DNA loop extrusion by condensin. *Science.* 360:102–105. https://doi.org/10.1126/science.aar7831.
47. Fudenberg, G., M. Imakaev, …, L. A. Mirny. 2016. Formation of chromosomal domains by loop extrusion. *Cell Rep.* 15:2038–2049. https://doi.org/10.1016/j.celrep.2016.04.085.
48. Nuebler, J., G. Fudenberg, …, L. A. Mirny. 2018. Chromatin organization by an interplay of loop extrusion and compartmental segregation. *Proc. Natl. Acad. Sci. USA.* 115:E6697–E6706. https://doi.org/10.1073/pnas.1717730115.
49. Goloborodko, A., M. V. Imakaev, …, L. Mirny. 2016. Compaction and segregation of sister chromatids via active loop extrusion. *Elife.* 5:e14864. https://doi.org/10.7554/elife.14864.